

www.acsami.org Research Article

# Accelerated Engineering of Optimized Functional Composite Hydrogels via High-Throughput Experimentation

Yang Liu, Junru Zhang, Yujing Zhang, Hu Young Yoon, Xiaoting Jia, Maren Roman, and Blake N. Johnson\*



Cite This: ACS Appl. Mater. Interfaces 2023, 15, 52908-52920



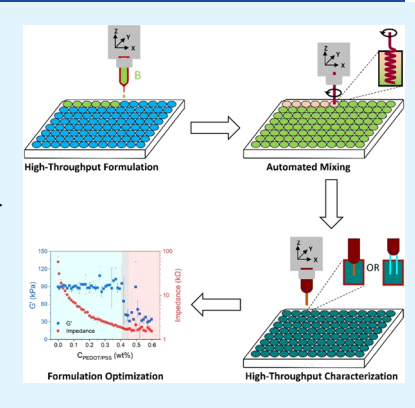
**ACCESS** I

Metrics & More

Article Recommendations

Supporting Information

ABSTRACT: The Materials Genome Initiative (MGI) seeks to accelerate the discovery and engineering of advanced materials via high-throughput experimentation (HTE), which is a challenging task, given the common trade-off between design for optimal processability vs performance. Here, we report a HTE method based on automated formulation, synthesis, and multiproperty characterization of bulk soft materials in well plate formats that enables accelerated engineering of functional composite hydrogels with optimized properties for processability and performance. The method facilitates rapid high-throughput screening of hydrogel composition-property relations for multiple properties in well plate formats. The feasibility and utility of the method were demonstrated by application to several functional composite hydrogel systems, including alginate/poly(N-isopropylacrylamide) (PNIPAM) and poly(ethylene glycol) dimethacrylate (PEGDMA)/poly(3,4-ethylenedioxythiophene)poly(styrenesulfonate) (PEDOT:PSS) hydrogels. The HTE method was leveraged to identify formulations of conductive PEGDMA/PEDOT:PSS composite hydrogels for



optimized performance and processability in three-dimensional (3D) printing. This work provides an advance in experimental methods based on automated dispensing, mixing, and sensing for the accelerated engineering of soft functional materials.

KEYWORDS: Materials Genome Initiative, high-throughput characterization, high-throughput synthesis, sensing, soft robotics

# 1. INTRODUCTION

The Materials Genome Initiative (MGI) aims at accelerating the pace of materials discovery, engineering (e.g., optimization), and commercialization while minimizing resource expenditures through innovation in materials research infrastructure. Creating new experimental tools and methods for rapid experimentation, which includes formulation, synthesis, and characterization, remains a critical bottleneck. Highthroughput experimentation (HTE) is foundational to accelerating the pace and impact of simulation, such as through model validation and support of digital twin, and also provides a direct path to experimentation-based accelerated materials discovery in the absence of simulation. HTE is now central to the pharmaceutical industry and other industries and fields based on molecular engineering and technology and is presently evolving to support accelerated materials discovery and engineering. For example, HTE for thin-film materials research, driven by the translatability of existing processes and analytical techniques for thin-film synthesis and characterization, has received considerable attention to date. Associated HTE methods for thin-film systems have been applied to a range of applications, based on electronic, magnetic, optical, and energy-related materials. 1,3

Compared with hard materials, relatively less progress has been made in the HTE of soft materials (e.g., hydrogels) due to challenges associated with adapting conventional methods for formulation, synthesis, and characterization of soft materials to high-throughput formats. However, stemming from progress in rapid prototyping (e.g., via additive manufacturing), new methods for high-throughput formulation and synthesis of soft materials are now emerging, such as for the high-throughput synthesis (HTS) and high-throughput characterization (HTC) of hydrogels. Microfluidics now serves as a common HTE format for accelerated hydrogel engineering. For example, Kumachev et al. recently reported a microfluidic approach for HTS of hydrogel microbeads with varying elasticities for cell encapsulation.4 While microfluidicbased formats exhibit several attractive characteristics, such as continuous production modality, they are relatively limited regarding ease of interface with HTC (i.e., the characterization of materials generated via microfluidic-based HTE formats presents a bottleneck).5,6 Robotic dispensing, commonly in microarray geometry, also provides another HTE format for accelerated hydrogel engineering. In this method, hydrogel precursor solutions are typically deposited on a substrate in a

Received: August 3, 2023 Revised: October 11, 2023 Accepted: October 18, 2023 Published: October 31, 2023





dropwise manner, such as via inkjet printing, enabling the formulation of a "library" of hydrogel samples via spatial control of the deposited volume of each component (e.g., precursor solution or cross-linking agent).7-10 Fabrication of functionally graded materials has also emerged as a method for accelerated engineering of hydrogels, 11,12 but is relatively constrained regarding interface with HTC methods, as the method does not produce a large number of samples. While several useful HTE formats for accelerated engineering are emerging, quality assurance and quality control remain critical areas such as verification of component mixing. In addition, formats based on microfluidics and microarray typically generate microscale samples, which may complicate the translation of generated process-composition-structureproperty relations to the design of macroscale constructs (e.g., soft robotics) and present challenges associated with benchmarking with established characterization data or results obtained from simulation of bulk material behavior. Toward addressing these challenges, integrated robotic dispensing and molding processes have served as an attractive format for accelerated hydrogel engineering. 13,14 Compared with microfluidic, microarray, and graded materials-based methods, the format generates large quantities of bulk samples in substrates (e.g., well plates) that synergize with a range of HTC methods. However, it remains a challenge to execute HTC of disparate properties from large batches of synthesized samples with varying compositions (i.e., hydrogel libraries) such as physical or mechanical properties that are essential for assessing and optimizing both processability and performance.

HTC methods can be broadly characterized as based on microfluidics, arrays, or robotics. 5,6,8,9,13 While several HTC methods exist for hard thin materials, often based on adapted spectroscopic methods, fewer exist for HTC of bulk soft materials. In particular, HTC of bulk soft material mechanical properties in conventional high-throughput formats, such as well plates, remains a challenge. 15 As a result, characterization data for critical properties that inform hydrogel processability and performance are sometimes generated by selecting representative samples from the library, which have several limitations. The challenge originates from the limited throughput associated with conventional characterization methods for hydrogels (e.g., dynamic mechanical analysis) and the incompatibility of the sample geometry among emerging HTS methods and established characterization methods. For example, microparticle geometries generated by microfluidic- and microarray-based formats are often incompatible with traditional rheological measurements. 4,10,16 Likewise, traditional characterization methods (e.g., atomic force microscopy) may require sample immobilization on a substrate.1 Thus, optical-based HTC methods, such as based on fluorescence spectroscopy or image analysis, are commonly used to characterize large batches of hydrogel samples produced via HTS. To address these limitations, new HTC methods for hydrogels are continuing to emerge. For example, Andre et al. reported a new approach for characterizing the viscoelastic properties of droplets by shape analysis.<sup>18</sup> Oevreeide et al. described the potential to characterize microgel mechanics in microchannels. 19 Marquez et al. developed an indentation system for HTC of hydrogel tissue construct mechanics, while Xu et al. used a commercial indenter for HTC of hydrogel swelling characteristics and mechanical properties. 13,20 Zhang et al. recently established a method for HTC of hydrogel rheological properties in 96-well

plate formats via robotically directed sensing using piezo-electric milli-cantilever (PEMC) sensors. 15,21-24 However, there remains a need for HTE formats capable of integrated high-throughput formulation, HTS, and HTC of complementary multiproperty information that can support the accelerated engineering of functional composite hydrogels with optimized processability and performance, particularly in practical cross-disciplinary formats, such as well plates.

In our previous work, we established a HTC platform for characterization of solution and hydrogel rheological properties in well plate formats. 15 Here, we establish a HTE method based on automated sample preparation (i.e., dispensing, mixing, and synthesis) and multiproperty characterization in standard 96-well plate formats. We focus on the processing of hydrogel precursor solutions across a wide viscosity range. The HTE method is leveraged to identify formulations of several functional composite hydrogels that exhibit optimized processability and performance.

#### 2. EXPERIMENTAL SECTION

2.1. Materials. Poly(ethylene glycol) dimethacrylate (PEGDMA,  $M_n = 750$ ), 2,2-dimethoxy-2-phenylacetophenone (DMPA), alginic acid sodium salt, calcium chloride (CaCl<sub>2</sub>), N-isopropylacrylamide (NIPAM), N,N'-methylenebis(acrylamide) (MBAA), and poly(3,4ethylenedioxythiophene)-poly(styrenesulfonate) (PEDOT:PSS, 1.3 wt %) were purchased from Sigma-Aldrich. Lead zirconate titanate (PZT-5A,  $72.4 \times 72.4 \times 0.127 \text{ mm}^3$ ) with nickel (Ni) electrodes was obtained from Piezo Systems (Woburn, MA). Glass cylinders and ethanol (200 proof) were from Fisher Scientific. Polyurethane (Fast-Drying) and Loctite EA 1C-LV epoxy adhesive were from Minwax and Henkel, respectively. Deionized water (DIW) (18.2 M $\Omega$ ) was from a DIW system (Direct-Q 3 UV Water Purification Systems; Millipore).

2.2. Automated High-Throughput Formulation and Synthesis of Hydrogels via Robotically Directed Multimaterial Dispensing and Mixing. Hydrogel stock precursor solutions were dispensed using a custom robot-assisted liquid dispensing system composed of a robot (F5200N; FISNAR) and a dispensing system (Ultimus V; Nordson EFD). The viscosities of the processed solutions were measured by a digital rotational viscometer (ViscoQC 100; Anton Paar) at room temperature. The precursor solutions were dispensed from a syringe barrel (55 or 10 mL) using a straight cylindrical nozzle (32 or 27 gauge). For a given stock precursor solution, the mass of dispensed solution was controlled by the dispensing pressure, dispensing time, and size of the dispensing nozzle, which ranged from 1.9-27.3 kPa, 0-47.5 s, and 32-27 gauge, respectively. The dispensing parameters were selected to achieve a linear relationship between the mass of the dispensed solution and the dispensing time per well prior to each experiment to ensure composition control for each sample (dispensing times for the different precursor solutions are described in the following sections). Here, the lower threshold was set as 0, and the upper threshold was set based on the dynamic range of the sensor (i.e., the concentration at which the cantilever quality factor drops below the threshold required for resonance tracking). We note that depending on the level of knowledge associated with the material system under investigation, the concentration ranges for individual components could be selected based on prior knowledge. In the cases of accelerated materials discovery applications in which limited information may exist about the interaction among individual components or resultant material properties (e.g., phase behavior), several rounds of HTE may be required to narrow the design space to a feasible range. The number of samples and resolution of the composition-property relations (i.e., step size in the concentrations of individual components) are also user-defined parameters that may be influenced by the application. Here, the formulation was performed in commercial 96- and 48-well plates to demonstrate that the automated dispensing process is compatible with conventional platforms for HTE. The robot path

associated with the automated formulation corresponded to a 96- or 48-point dispense command that was executed in an *N*-shaped path that corresponded to the dimensions (e.g., well spacing) of the given well plate. The dispense time (i.e., dwell time) per well varied for each solution and desired mass dispensed. The movement speed of the dispensing nozzle between each well was 10 mm/s. A new dispensing nozzle was used for each experiment.

2.2.1. Automated Mixing. Following the dispensing process and prior to the cross-linking (i.e., synthesis) process, the dispensed components in each well were mixed by various strategies, including diffusion, a digital plate shaker (LSE digital microplate shaker; Corning), and robotically directed mixing. Hydrogel libraries that contained alginate-based precursor solutions, which were relatively viscous, were mixed by a robot-assisted mixing method, using the same dispensing robot. The mixing pattern in each well was controlled by using a circular band motion command, which generated a spiral path for mixing with a given brush area. The mixing time varied between 30 and 75 s. The gap between the stirrer and the bottom of the well plate was 0.1 mm. Stir tools with straight cylindrical geometry (22, 20, and 18 gauge nozzles) and helical geometry (steel wire (diameter (d)  $\sim 0.4$  mm); inner helix d = 1.4, 1.7, and 2.0 mm; pitch ~1.5 mm) were fabricated and affixed to unfilled dispensing barrels to facilitate robotically directed mixing (see Figure S1). Hydrogels that contained relatively less viscous precursor solutions with viscosities similar to DIW were mixed by a digital shaker at 1000 rpm for 2 min. Photographs of the mixed samples were acquired before and after mixing.

2.2.2. PEGDMA Hydrogels. A PEGDMA stock solution was prepared by dissolving 4.5 g of PEGDMA in 24.73 mL of DIW, followed by mixing with 0.77 g of 1 wt % DMPA solution in ethanol, which resulted in a stock precursor solution that contained 15 wt % of PEGDMA and 0.5% DMPA with respect to the PEGDMA molar concentration. The stock solution was then filtered through a 0.45  $\mu m$ nylon syringe filter to remove large particles. 96-Well plates were used as reaction vessels for high-throughput formulation, synthesis, and characterization. The precursor solution was dispensed using a straight cylindrical nozzle (32 gauge). The 96 samples were formulated with the PEGDMA stock solution by using a dispensing time (i.e., dwell time) per well that ranged across the plate from 0 to 47.5 s, with a step size of 0.5 s. To complete the formulation of the hydrogel library, DIW was dispensed in the opposite path direction (i.e., beginning in the last well and traveling to the first well) with dwell time ranging from 47.5 to 0 s, with a step size of 0.5 s. After dispensing, the samples were mixed with a digital shaker at 1000 rpm for 2 min prior to cross-linking. The PEGDMA hydrogels were then obtained by exposure of the samples (i.e., well plate) to UV light for 30 min (365 nm; UVGL-58; Analytik Jena US LLC).

2.2.3. Alginate/PNIPAM Hydrogels. A 2 wt % alginate precursor solution was obtained by dissolving alginic acid sodium salt in DIW. A 100 mM CaCl<sub>2</sub> in DIW served as the stock cross-linking solution. The PNIPAM precursor solution was prepared by dissolving NIPAM and MBAA in DIW, followed by mixing with 16  $\mu$ L of 1 wt % DMPA solution in ethanol, which resulted in a stock precursor solution that contained 6.7 wt % of NIPAM in which the molar ratio between NIPAM, MBAA, and DMPA was 1:0.005:0.0005, respectively. The NIPAM and CaCl<sub>2</sub> solutions were separately filtered with a 0.45  $\mu$ m nylon syringe filter prior to dispensing. The alginate precursor solution was first dispensed using a straight cylindrical nozzle (27 gauge) for a dispense time of 10 s in each well. Then NIPAM solution was then dispensed using a straight cylindrical nozzle (32 gauge) for a dispense time that ranged from 0.5 to 48 s, with an increment of 0.5 s per well. DIW was dispensed in an opposite path direction for a dispense time that ranged from 48 to 0.5 s to achieve a constant total mass in each well. The samples were then mixed via robotically directed mixing for 56 s per well using the helical stirring tool. The samples (i.e., well plate) were then exposed to UV light (365 nm) for 30 min to polymerize the PNIPAM network of the composite hydrogel. Finally, 30.7 mg of CaCl<sub>2</sub> solution was dispensed on the surface of each sample using a circular band path trajectory to chemically cross-link the alginate network of the composite hydrogel. The alginate/PNIPAM composite hydrogels were then obtained by allowing the cross-linking reaction to proceed for 12 h in a humid environment.

2.2.4. PEGDMA/PEDOT:PSS Hydrogels. A stock PEGDMA precursor solution (25 wt %) was first dispensed using a straight cylindrical nozzle (27 gauge) for 3 s in each well. The vendor-provided PEDOT:PSS formulation (1.3 wt %) served as the PEDOT:PSS precursor solution and was then dispensed in each well with a dispense time of 0 to 23.5 s and a step size of 0.5 s. The stock DMPA precursor solution in ethanol (10 wt %) was then dispensed for 3 s in each well. The precursor solution was then mixed with a digital shaker at 500 rpm for 5 min. Finally, the precursor solution was photopolymerized by exposure to UV light (365 nm) for 45 min.

**2.3.** Automated HTC of Hydrogel Properties in Well Plate Formats. Multiple properties of the synthesized hydrogel libraries, including mechanical, optical, and electrical properties, were characterized in well plate formats by using various automated HTC techniques.

2.3.1. HTC of Hydrogel Rheological Properties. Rheological properties of the synthesized hydrogel libraries were characterized in high throughput via robotically directed sensing using PEMC sensors (see Figure S1) and a recently reported method. 15 The PEMC sensor fabrication method and measurement principle can be found in our previous reports.<sup>21–25</sup> PEMC sensor phase angle at resonance, which correlates with the material shear storage modulus (G'),  $^{21}$ was continuously monitored using an impedance analyzer (e5061b; Keysight) and custom Matlab program for data acquisition. The path planning parameters for HTC in 96-well formats, which included a 30 or 60 s dwell time per well, is provided in our recent report. 15 Rheological property characterization data and the corresponding heat maps are presented as the steady state of the phase angle at resonance in each material (i.e., well). After all samples were characterized, the sensor signal was acquired in air for 30 min to reestablish the sensor baseline after testing.

2.3.2. HTC of Hydrogel Electrical Properties. The electrical properties of the synthesized hydrogel libraries were characterized via robotically directed sensing using a robot (F5200N; Fisnar) and an impedance analyzer (e5061b; Keysight). Electrochemical impedance spectroscopy (EIS) was performed at 3 kHz with zero DC bias using a two-electrode setup (see Figure S1; electrode 1 = platinum (d = 1 mm; Sigma); electrode 2 = platinum (d = 0.25; Alfa Aesar)). The electrode separation distance was 4 mm. The path trajectory and path planning parameters were identical to those used for HTC of the rheological properties. EIS characterization data are presented as the steady-state electrical impedance (Z) in each well. The electrical impedance obtained using the impedance analyzer was benchmarked against a potentiostat (Interface 1000; Gamry) by collecting EIS data across the 0.1-100 kHz frequency range using a two-electrode setup, identical electrodes, and a stimulus of 10 mV AC and zero DC bias. The electrical impedance at 3.144 kHz was used for benchmarking.

The conductivity  $(\sigma)$  of the samples was obtained using an electrometer (Keithley 6514; Tektronix) using a custom mold (width (W)=4 mm; height (H)=3 mm; length (L)=40 mm) and a parallel plate (copper) electrode configuration, which yielded the resistance (R). Multiple measurements were performed at three different sample lengths (20, 30, and 40 mm) to verify that the contact resistance  $(R_{\text{contact}} < 1\% R)$  was neglectable compared to the bulk resistance. The conductivity was calculated as  $\sigma = L/(RWH)$ .

2.3.3. HTC of Hydrogel Optical Properties. Optical properties, specifically absorbance (A) at 450 nm, of the synthesized hydrogel libraries were measured by using a microplate reader (Synergy H1; BioTek Instruments). Measurements were first obtained at room temperature and subsequently at 37  $^{\circ}\text{C}$  by immersing the well plate in a water bath until the samples reached thermal equilibrium, after which the absorbance was measured.

**2.4.** Three-Dimensional (3D) Printing of Conductive Hydrogels with Optimized Formulation. The formulation of the PEGDMA/PEDOT:PSS composite hydrogel for optimized processability and performance identified by HTC of mechanical and

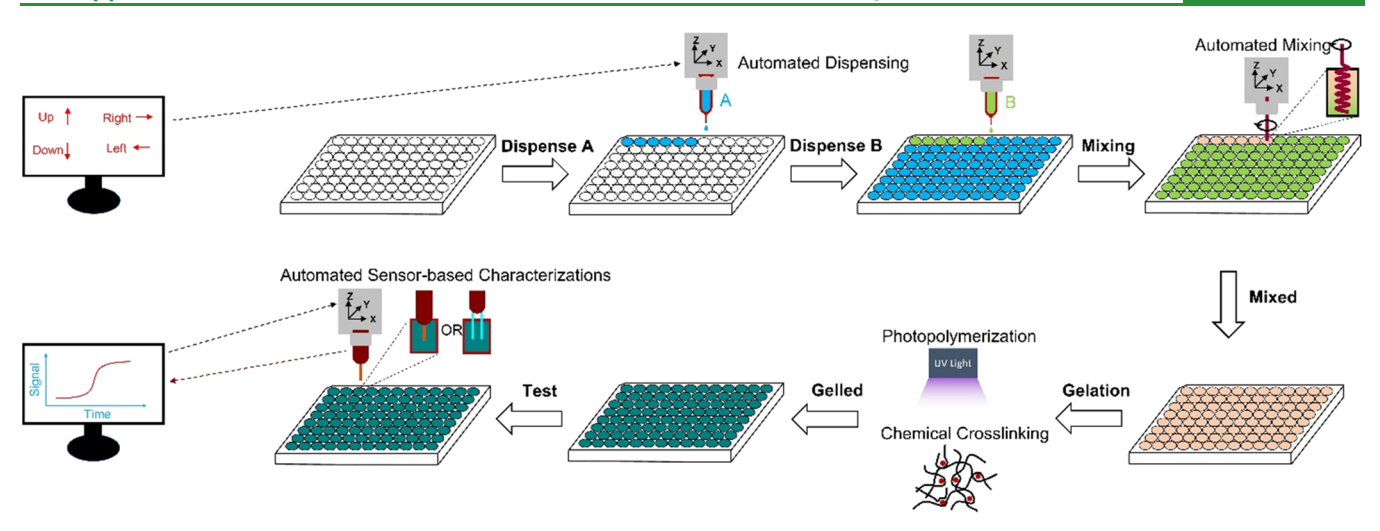


Figure 1. Schematic of the high-throughput experimentation (HTE) method for accelerated engineering of functional composite hydrogels with optimized properties for processability and performance via robotically directed multimaterial formulation, synthesis, and multiproperty characterization in well plate formats.

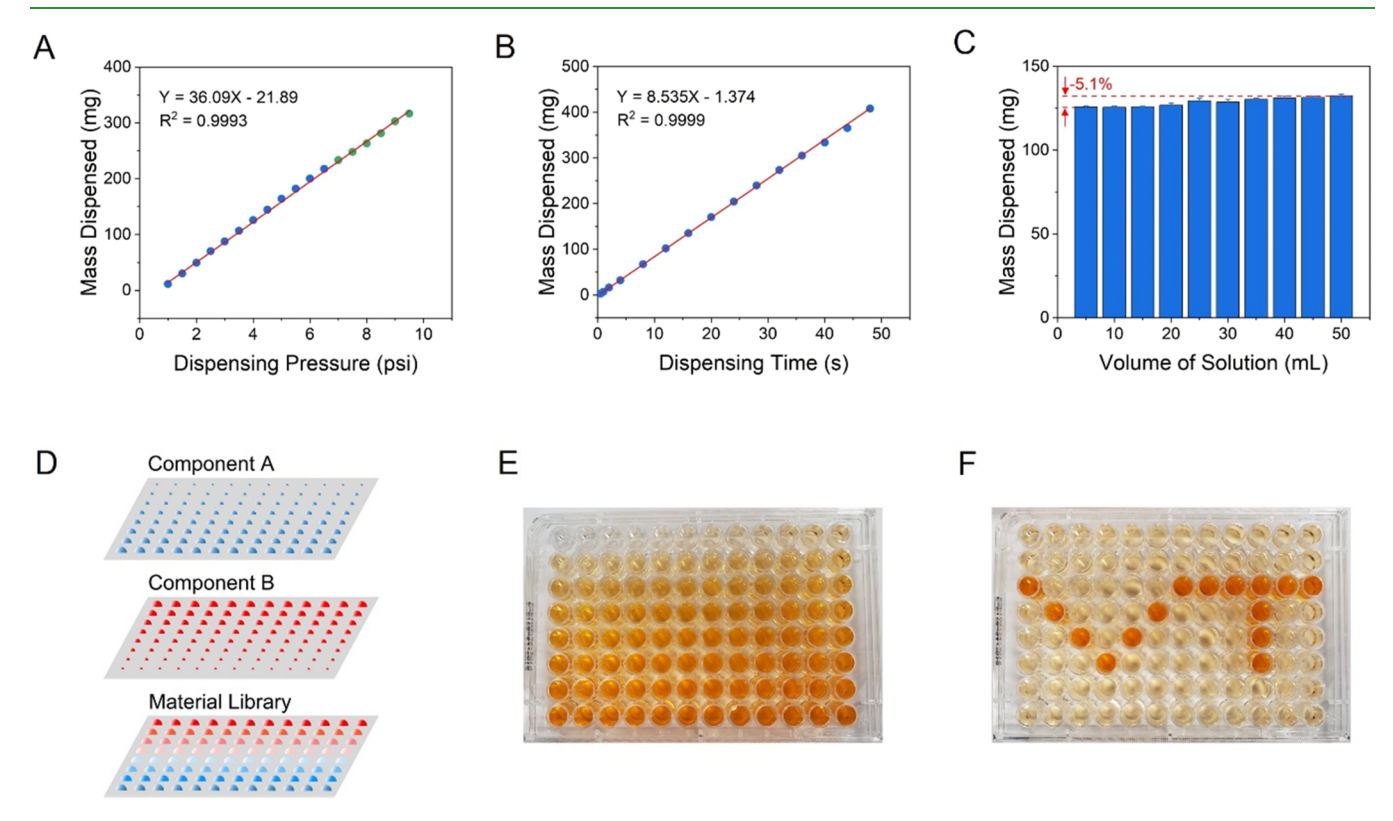


Figure 2. Relationship between the mass of dispensed solution and dispensing pressure at a constant dispensing time (A) and dispensing time at a constant dispensing pressure (4 psi) (B) (blue and green points represent droplet-based and continuous-flow dispensing regimes, respectively). (C) Effect of volume decrease in the dispensing container during formulation on the mass dispensed at constant dispensing pressure and time (4 psi and 15 s, respectively). Volume decreases in this study ranged from 0.3 to 18.3 mL. (D) Illustration of formulating a batch of hydrogel samples of varying composition via spatially controlled multimaterial dispensing. Photographs representing formulated hydrogel libraries in a 96-well plate format using an orange dye with a linear distribution in mixture composition (E) established by the method shown in panel (D) and a nonlinear distribution in mixture composition (F).

electrical properties, respectively (i.e., the formulation that provided a balance of G' and conductivity  $(\sigma)$ ), was utilized for 3D printing. The optimized precursor solution formulation contained 13.1 wt % PEGDMA, 0.4 wt % PEDOT:PSS, and 0.2 wt % DMPA. Silicone support structures were printed in the shape of a Virginia Tech logo (i.e., adjacent "V" and "T" characters) on a glass slide. The optimized precursor solution was then printed layer by layer in the support structure. After each layer was printed, the dispensed solution was

cured by exposure to a UV light (365 nm) for 10 min. The cured composite hydrogel construct was then removed from the support structure. The two electrodes of a light-emitting diode (3–3.2 V forward voltage; MCIGICM) were then inserted in the constructs (i.e., one electrode was inserted into each character; the characters were otherwise not in contact). Copper wires under each of the characters (one per character) served as the interconnect to a direct current (DC) power supply (GPD-2303S; GW Instek). The copper

interconnects contacted only the bottom surface of the hydrogel to avoid direct contact with the light-emitting diode (LED) electrodes that penetrated the top surface of the hydrogel. Photographs of the circuit composed of the LED and conducting composite hydrogel were obtained between 5 and 8 V. A second circuit composed of LEDs and cured composite hydrogel constructs was also fabricated. Multiple rectangular constructs ( $13 \times 7 \times 2 \text{ mm}^3$ ) were prepared by molding. The constructs and five LEDs were then connected in series in an alternating configuration to form a "V" character. The bottom surfaces of the two terminal hydrogel constructs were contacted with copper foil to facilitate the connection to the DC power supply. Photographs of the circuit composed of the five LEDs and hydrogel interconnects were obtained between 14 and 16 V.

**2.5. Data Analysis.** All experiments were repeated at least three times. The reported results correspond to the mean and standard deviation of all experiments. Details associated with conversion of PEMC sensor data to mechanical property information (i.e., G') can be found in our previous work and the Supporting Information. <sup>21,24</sup>

# 3. RESULTS AND DISCUSSION

3.1. High-Throughput Formulation of Hydrogel Libraries via Robotically Directed Multimaterial Dispensing. While several reports have been made on HTS and HTC, 4,6-14 it remains a goal to establish integrated HTS and HTC processes that can autonomously operate in a closed loop with minimal human intervention (e.g., manual operations or human decision-making). In addition, there remains a need for accelerated materials discovery workflows for functional soft materials that support both established and emerging areas, including tissue engineering and soft robotics, respectively. HTE requires three steps: formulation (i.e., selection and combination of components), synthesis (i.e., reaction of combined components), and characterization (i.e., analysis of the composition, structure, and properties of resultant product mixtures). As shown in Figure 1, here, we provide an automated HTE method for accelerated engineering and optimization of soft functional composite hydrogels based on robotically directed dispensing and sensing.

We first demonstrated that robotically directed dispensing enables high-throughput formulation of hydrogels by controlled integration of precursor solutions, cross-linking agents, and associated solvents (e.g., DIW). As shown in Figure 2A and B, respectively, the mass of the dispensed liquid increased linearly with respect to the dispensing pressure and time. The method provided two dispensing regimes across the investigated pressure range, specifically a droplet-based regime and a continuous-flow regime. A dispensing pressure of 6.5 psi was the transition point of the two regimes. Linear relationships between the dispensed mass, dispensing pressure, and time were consistent across the two regimes. Given that the volume of liquid in the dispensing container (i.e., syringe) decreases throughout the formulation process, we next investigated the influence of the dispensed liquid volume on the dispensed mass. As shown in Figure 2C, we found that the process enabled controlled dispensing as the volume of the dispensing container decreased. Figure 2C shows that the change in mass dispensed associated with the volume decreases that occurred during the high-throughput formulation studies in this work, which ranged from 0.3 to 18.3 mL, was minimal and quantifiable.

As shown in Figure 2D, a batch of samples with varying mixture compositions, termed a library, can be formulated by successive dispensing of multiple stock solutions that exhibit different components or concentrations in varying spatial

distributions and volumes across a well plate. The stock solutions can represent precursor solutions, cross-linking agents, or solvents. Figure 2D illustrates the process of formulating a hydrogel library by dispensing two solutions such as a concentrated precursor solution and a diluent. For example, component A is dispensed from low to high mass across the well plate with respect to ascending well number, while component B is dispensed from low to high mass in the opposite path direction (i.e., with respect to descending well number). The process was demonstrated using a dyecontaining solution and DIW, which represent components A and B, respectively (Figure 2E). The ability to control the mass of the dispensed solutions across a 96-well plate in nonlinear spatial distributions was demonstrated in Figure 2F by formulating a Virginia Tech logo (i.e., "V" and "T" characters).

3.2. Automated Mixing of Formulated Hydrogel Libraries Containing Viscous Precursor Solutions. In addition to the automated formulation of batches of samples with varying mixture compositions, mixing of the formulated samples is a critical aspect of HTS, particularly when considering accelerated discovery and optimization of bulk materials. For example, HTS of material libraries that contain samples with spatially nonuniform distributions of reactants may affect the accuracy and fidelity of composition-structureproperty relations that are obtained via subsequent HTC. Given that composite hydrogels are often synthesized by combining several precursor solutions, cross-linking agents, and solvents, which may exhibit different densities and viscosities, validation of mixture mixing is an important step associated with HTS of composite hydrogels. While mixing may be achieved by diffusion in microarray- and microfluidicbased formats for the HTS of hydrogels, it may be insufficient for the HTS of bulk composite hydrogels. Thus, additional mixing techniques, such as shaking 13 and sonication, 14 have been implemented for HTS applications in well plate formats. At present, most reported studies on HTS of hydrogels have utilized precursor solutions of relatively low viscosity similar to DIW. However, the use of relatively high-density and highviscosity precursor solutions increases the demand for both establishing novel in situ mixing techniques and validating sample mixing prior to synthesis steps. Multimaterial printing processes that require mixing of printed materials may be accomplished in-line, 26 but also be constrained by sample size, discrepancy of the printed material rheological properties, and kinetics of hydrogel gelation. While in-line mixing of dispensed or printed components prior to deposition has opportunities for creating blends and gradients in material composition throughout a construct, in-line mixing techniques based on static mixers have the drawback of a material residence time, which limits low-volume applications. Here, we did not constrain processing in the well plate format with in-line mixing strategies during dispensing based on the synergy of well plates with various mixing processes. Thus, we next examined a well plate-compatible robotically directed highthroughput mixing technique and benchmarked the performance (i.e., mixing time and efficiency) vs standard mixing techniques of diffusion and plate shaking.

A comparative study was performed by observing the mixing between a viscous and an inviscid precursor solution, represented by an alginate/PEDOT:PSS precursor solution and DIW, respectively. Alginate/PEDOT:PSS solution (100  $\mu$ L; 2 wt %) was first added to a well, followed by DIW (290

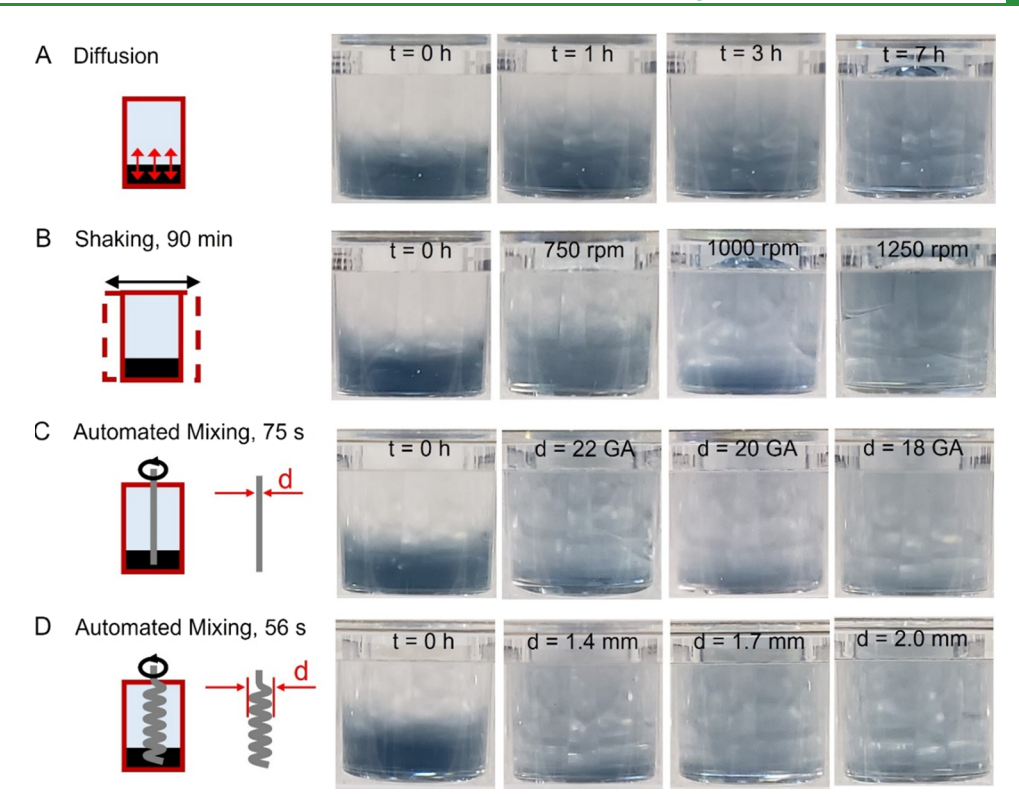


**Figure 3.** Comparison of a robotically directed mixing method with established methods using a viscous alginate/PEDOT:PSS precursor solution and a diluent. (A) Photographs of the mixing efficiency achieved by diffusion for 1, 3, and 7 h. (B) Photographs of the mixing efficiency achieved by a digital plate shaker for 90 min at 750, 1000, and 1250 rpm. (C) Photographs of the mixing efficiency achieved by robotically directed mixing for 75 s with a straight cylindrical stirring tool (22, 20, and 18 gauge nozzles). (D) Photographs of the mixing efficiency achieved by robotically directed mixing for 56 s with a helical stirring tool (d = 1.4, 1.7, and 2.0 mm).

 $\mu$ L). The viscosity of the 2 wt % alginate stock solution used in this research was 977.9 mPa s. As a comparison, 25 wt % PEGDMA aqueous solution, which exhibits a viscosity similar to many common precursor solutions, was 11.9 mPa s. The viscosities of several other solutions used in this work are also provided in Table S1 of the Supporting Information. As shown in Figure 3A, diffusion was unable to rapidly establish a uniform mixture (i.e., a mixture with a uniform spatial distribution of components). In contrast, plate shaking for 90 min established a uniform mixture (Figure 3B). Similarly, we found that robotically directed mixing for approximately 1 min per well also established a uniform mixture. Figure 3C and 3D compare the effect of the stirring tool geometry on the required mixing time. We found that the required time to achieve a uniform mixture correlated with the surface area of the stirring tool, which is consistent with a drag-based mixing mechanism. Given that the robotically directed mixing method required ~1 min per well, the total mixing time and quality were comparable to plate shaking; however, we note that multiplexed stirring tools may be developed that facilitate simultaneous mixing of multiple wells, which can potentially reduce the mixing time for the library to as low as 1 min, which would be a significant improvement relative to plate shaking. In practice, the mixing method utilized (e.g., diffusion, plate shaking, robotically directed mixing) is likely application- and material-dependent (e.g., dependent on required throughput and properties of integrated components, respectively). However, it is critical to examine methods that can potentially decrease the cycle time associated with the mixing process as well as to validate that samples generated by high-throughput formulation processes exhibit uniform mixtures prior to

synthesis. Efficiency is also important for high-throughput experimentation, as effective mixing of reagents prior to, and sometimes during, the reaction is a critical aspect of creating sample quality and reproducibility. Overall, there is a goal to optimize the efficiency (i.e., reduce cycle times) of formulation, mixing, reaction, and characterization processes to improve the cycle rate of high-throughput experimentation processes. The choice of mixing technique is dependent on various factors, including the differences in density, viscosity, and miscibility of dispensed solutions, the relative rates of phase separation (if any) and reaction, sample size, cross-linking method and parameters, and required sample quality. Here, our goal was to demonstrate that a combination of viscous and inviscid solutions or suspensions in a well plate format by multimaterial dispensing can be actively mixed following dispensing, which could reduce the time-to-results relative to diffusive mixing or sonication.

**3.3.** HTC of Hydrogel Mechanical Properties. Having validated the high-throughput formulation process for HTS of hydrogels in well plate formats, we next demonstrated the integrated HTS and HTC of a highly utilized hydrogel system (PEGDMA hydrogel).<sup>27–29</sup> As shown in Figure 4A,B, the frequency response of a PEMC sensor across the 30–60 kHz frequency range, which contained a resonant mode, facilitates characterization of the hydrogel mechanical properties via a material—structure interaction mechanism. For example, as shown in Figure 4B, the sensor phase angle at resonance was dependent on the hydrogel's PEGDMA concentration. The raw data associated with HTC of the hydrogel library mechanical properties via robotically directed sensing are shown in Figure 4C. The sensor response associated with the

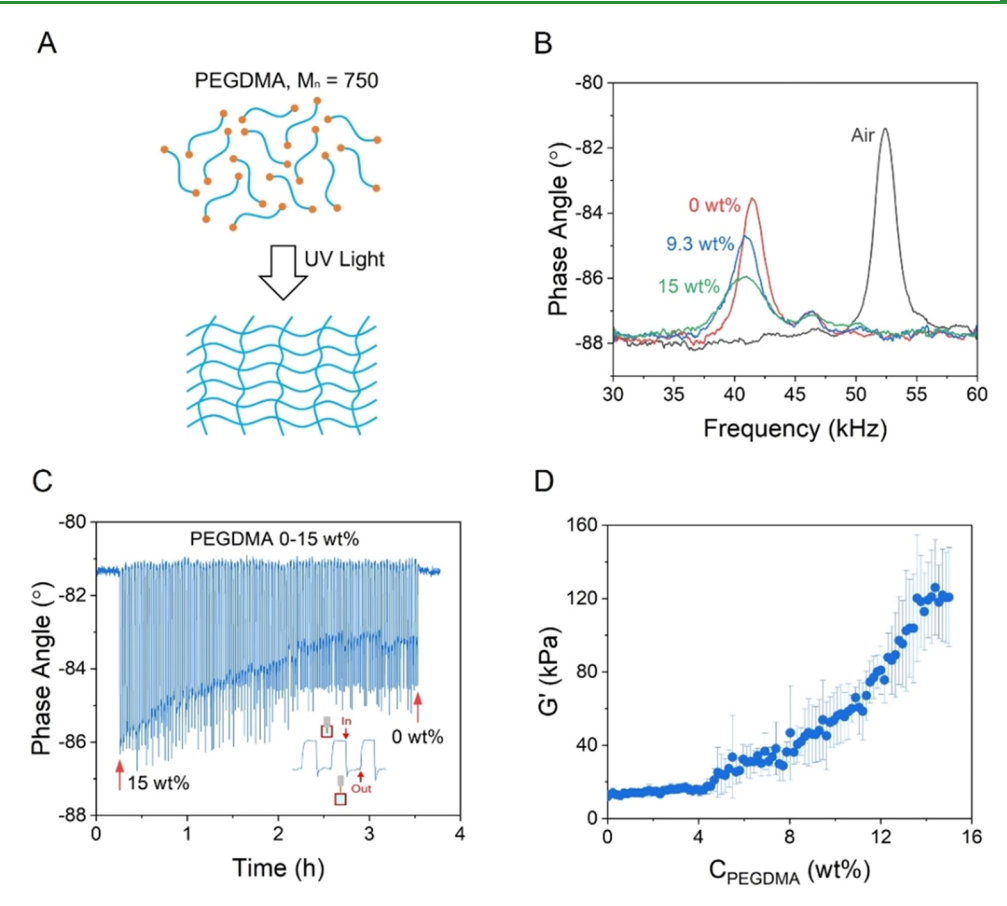


**Figure 4.** (A) Illustration of the photopolymerization process for PEGDMA hydrogel gelation. (B) Impedance spectra (phase angle response) of PEMC sensors across the 30–60 kHz frequency range in air, DIW, 9.3 wt % PEGDMA hydrogel, and 15 wt % PEGDMA hydrogel. (C) Real-time phase angle at resonance response (raw HTC data) associated with HTC of PEGDMA hydrogel mechanical properties in a 96-well plate format ranging from 0 to 15 wt %. (D) Generated composition—property relation data for the PEGDMA hydrogel in terms of shear storage modulus (G') dependence on PEGDMA concentration.

measurement of a single sample contains three phases: a penetration phase, a measurement phase, and a removal phase. A zoomed-in response of the sensor phase angle at resonance is shown in the lower right-hand corner of the panel, which highlights the measurement of three adjacent samples.

As shown in Figure 4C, the steady-state sensor phase angle at resonance in each sample exhibited a nonlinear decrease with respect to the PEGDMA concentration across the 0-15 wt % concentration range. Comparison of the sensor baseline before and after the study as well as before and after individual sample measurements indicates both minimal drift in the response and the absence of material adhesion during characterization of successive samples. The sensor baseline drift was examined as a negative control (see Figure S2). The sensor response recovered after each measurement cycle (i.e., penetration and removal event) to 99.97 ± 0.19% of the original baseline. The baseline drift ranging among multiple sensors was  $-0.08 \pm 0.17\%$  (n = 4 repeated tests using two different sensors), which was significantly lower than the signal change associated with the HTC studies (for example, Figure 2C). Figure 4D shows the composition-property relation generated from the raw HTC data using a fluid-structure interaction model $^{21,30}$  as a relationship between G' and PEGDMA concentration. The fluid-structure interaction model allows measurements of the sensor's resonant frequency and quality factor, which is correlated with the phase angle at resonance, to be converted to viscoelastic properties of the

surrounding materials. The correlation of the viscoelastic properties measured at the resonant frequency using the cantilever sensor with low-frequency values obtained with traditional rheology and dynamic mechanical analysis has been previously established. 21-23 The fluid-structure interaction model is further described in the Supporting Information. The nonlinear trend of G' vs PEGDMA concentration exhibits three regions with transition points near 4 and 14 wt %. Initially, G' increases gradually at a constant rate with increasing PEGDMA until the first transition point near 4 wt %, after which G' increases at a relatively higher rate with nonlinear dependence on PEGDMA concentration until G' ultimately stabilizes near 14 wt % (the second transition point). The first transition point is associated with gelation of the mixture, and the second is associated with a plateau in the hydrogel G'. Similar characteristics of the sol-gel transition have been reported in several hydrogels and composites.<sup>31,32</sup> Thus, the reported HTE method offers new opportunities for studying the phase behavior and composition-property relationships of hydrogels.

**3.4.** HTE with High-Throughput Multiproperty Characterization of Stimuli-Responsive Composite Hydrogels. Having established the ability to study the phase behavior of hydrogels using HTC of mechanical properties, we next extended the HTE method to characterization of composition—multiproperty relation data. The demand for accelerated discovery and engineering (e.g., optimization) of

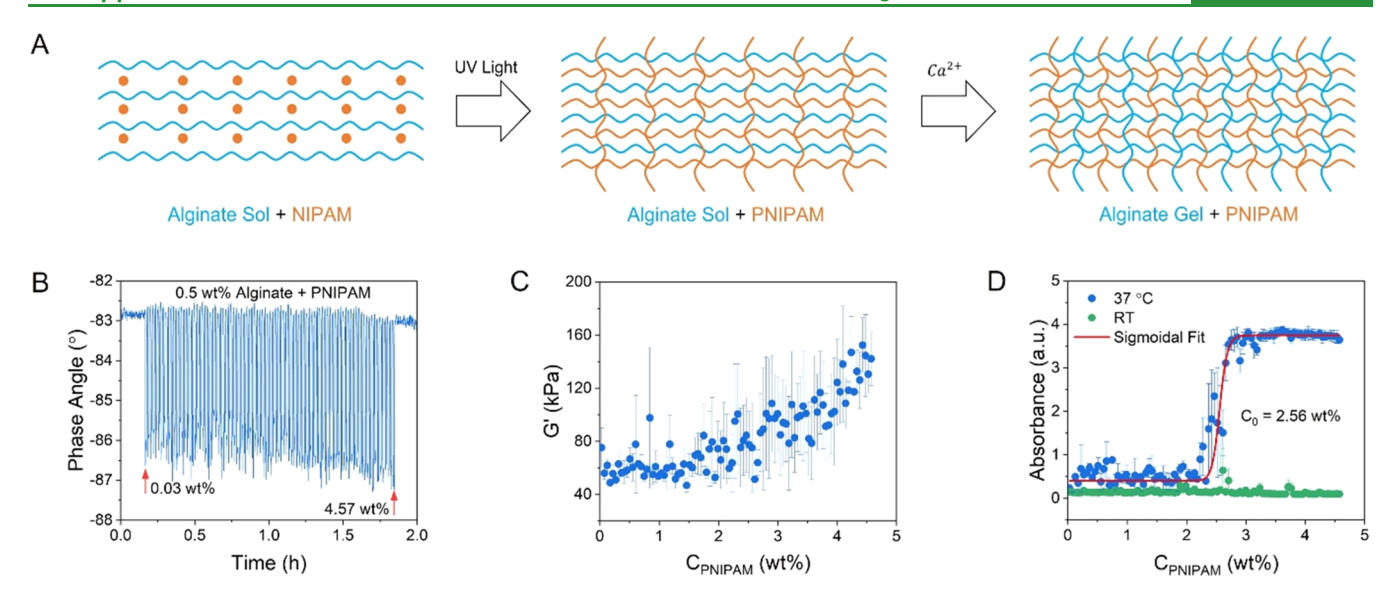


Figure 5. (A) Illustration of alginate/PNIPAM composite hydrogel formation via sequential photopolymerization of PNIPAM and chemical cross-linking of alginate. (B) Real-time phase angle at resonance response (raw HTC data) associated with HTC of alginate/PNIPAM composite hydrogel mechanical properties in a 96-well plate format. (C) Generated composition—mechanical property relation data in terms of PNIPAM concentration and G' of alginate/PNIPAM composite hydrogels. (D) Generated composition—optical property relation data in terms of PNIPAM concentration and absorbance (450 nm) of alginate/PNIPAM composite hydrogels below (room temperature) and above the LCST of PNIPAM (37  $^{\circ}$ C).

functional materials remains a driving force for the MGI. However, optimizing the formulation of functional materials requires multiproperty information to assess both functionality (i.e., performance) and processability. 33-35 Often, there is a trade-off between a material's processability and performance, and therefore, an optimized formulation should yield resultant properties that enable optimized processability and performance. Thus, we next examined the integration of complementary tools and methods for HTC of hydrogel optical and electrical properties with the established HTE method. Given the use of stimuli-responsive alginate/PNIPAM composite hydrogels for a range of applications, including soft robotics and 4D printing, and the ability to characterize the rheological properties of alginate/PNIPAM composite hydrogels using PEMC sensors,<sup>24</sup> we next leveraged the HTE method for multiproperty HTC of alginate/PNIPAM composite hydrogel libraries. Figure 5A illustrates the process of alginate/PNIPAM composite hydrogel formation. A mixture of alginate and NIPAM monomer solutions is first exposed to UV light to photopolymerize a PNIPAM network. Subsequently, the mixture is exposed to a Ca<sup>2+</sup>-containing solution to form an interpenetrated alginate network. The concentration of alginate in all samples was 0.5 wt %, while the concentration of PNIPAM varied from 0.03 to 4.57 wt %. Figure 5B shows the sensor phase angle at resonance response across the library, which exhibited a trend similar to that observed for the PEGDMA hydrogel library. The first transition point was observed near 2.5 wt % PNIPAM. The corresponding dependence of G' on the PNIPAM concentration is shown in Figure 5C and exhibited a similar trend. Likewise, the first transition point was observed near 2.5 wt % PNIPAM.

It is established that robust networks can enhance the strength of interpenetrated hydrogel networks.<sup>36</sup> While there are several methods to characterize the structure and properties of hydrogels, such as scanning electron microscopy (SEM), small angle neutron scattering (SANS), and rheometry,<sup>37–41</sup> most are incompatible with well plates. In

contrast, plate readers are mature well plate-compatible HTC platforms that are widely used for materials science, chemistry, biochemistry, and biology applications. 42-45 As shown in Figure 5D, the composite hydrogel exhibited relatively low absorbance at room temperature (RT) regardless of the PNIPAM concentration below the lower critical solution temperature (LCST) but exhibited a sigmoidal trend above the LCST, a characteristic of percolation. 46 When the PNIPAM concentration was below a threshold value (2.56 wt %), relatively weak absorbance was observed both below and above the LCST. The HTC data associated with the composite hydrogel optical properties (Figure 5D) was correlated with the HTC data associated with the composite hydrogel mechanical properties (Figure 5C) and can be utilized to interpret the composition-mechanical property relation data. For example, the data suggest that when the PNIPAM concentration was below 2.56 wt %, the covalent PNIPAM network was unable to reinforce the ionic alginate network, and the phase separation was weak when the temperature was above the LCST. In contrast, when the PNIPAM concentration was greater than 2.56 wt %, the PNIPAM network was capable of forming an effective interpenetrated network with the alginate network that both enhanced the mechanical properties and caused phase separation when the temperature was above LCST. Similar transitions have also been reported in other double-network hydrogels. 47,48 The results shown in Figure 5 suggest that the reported HTE method can potentially enable the accelerated engineering (e.g., optimization) of stimuli-responsive hydrogels for a range of applications. These results also demonstrate the value of leveraging complementary composition—property relations for data interpretation.

3.5. Accelerated Engineering of Optimized Functional Composite Hydrogels via HTE with High-Throughput Multiproperty Characterization. Having demonstrated the utility of the HTE method for understanding the phase behavior and formulation optimization of a stimuliresponsive composite hydrogel via multiproperty HTC, we

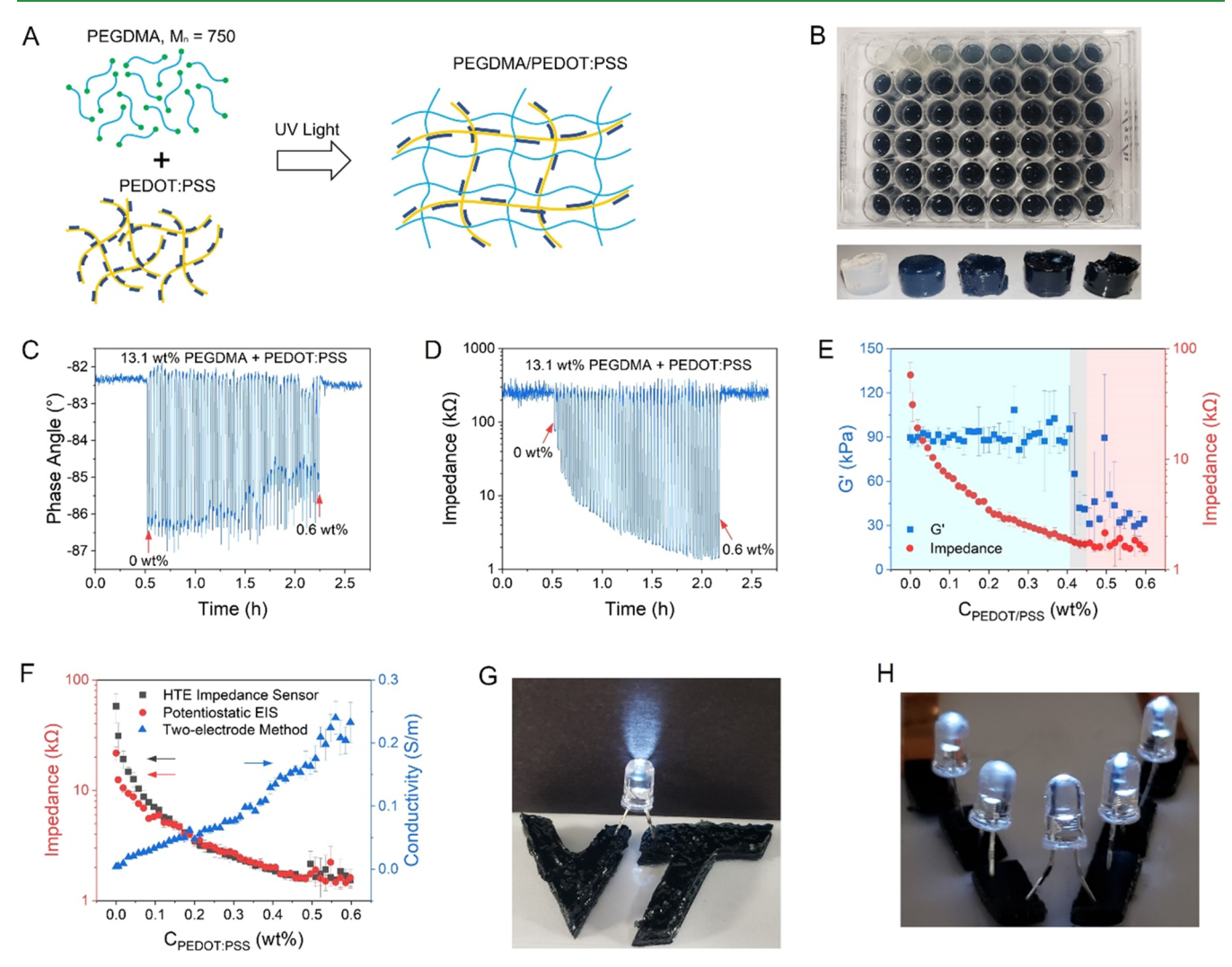


Figure 6. (A) Illustration of the formation of PEGDMA/PEDOT:PSS conductive composite hydrogels via photopolymerization. (B) Photographs of a formulated PEGDMA/PEDOT:PSS hydrogel library in a 48-well plate (upper panel) and representative samples containing 0, 0.09, 0.19, 0.36, and 0.56 wt % of PEDOT:PSS after manual removal from the well plate (lower panel). The samples highlight the brittleness of hydrogels composed of a relatively high PEDOT:PSS concentration (all samples exhibited consistent geometry before manual removal). Real-time phase angle at resonance response associated with HTC of mechanical (G'—panel (G') and electrical (impedance (G')—panel (G') properties of a 48-sample PEGDMA/PEDOT:PSS composite hydrogel library. (E) Composition—multiproperty relation data for the mechanical (i.e., G') and electrical (i.e., G') properties of PEGDMA/PEDOT:PSS composite hydrogels with respect to PEDOT:PSS concentration. (F) Composition—electrical property relation data in terms of electrical impedance obtained by multiple HTC methods and conductivity with respect to the PEDOT:PSS concentration. (G) Photograph of a 3D-printed PEGDMA/PEDOT:PSS composite hydrogel construct and integrated LED fabricated using an optimized formulation (13.1 wt % of PEGDMA and 0.4 wt % of PEDOT:PSS). (H) Photograph of multiple PEGDMA/PEDOT:PSS composite hydrogel constructs in series with five LEDs fabricated by using the optimized formulation.

next leveraged the method for understanding the phase behavior and formulation optimization of a conductive functional composite hydrogel. The conductive polymer PEDOT has been widely used for electronics applications. 49-52 However, the introduction of PEDOT, especially PEDOT:PSS particles, into another material may affect the mechanical properties of the resultant composite material and, thus, the performance and processability.<sup>53</sup> It remains a challenge to establish optimized formulations that may balance performance and processability metrics such as conductivity and elasticity. Thus, we next applied the HTE method with integrated multiproperty HTC to optimize a conductive functional composite hydrogel system, specifically, a PEGD-MA/PEDOT:PSS composite hydrogel (see Figure 6A). The PEGDMA concentration was constant at 13.1 wt % for all samples, while the PEDOT:PSS concentration increased from

0 to 0.6 wt %. A photograph of the library and representative samples after manual removal from the well are shown in Figure 6B. Visual inspection of representative samples removed from the well plate after synthesis revealed that increasing PEDOT:PSS concentration increased the sample brittleness, resulting in sample fracture by manual handling. Importantly, prior to removal and manual handling for photography purposes, all hydrogels exhibited similar geometry. Raw data associated with the rheological and electrical properties of the HTC process are shown in Figure 6C and D, respectively. As shown in Figure 6E, there was a trade-off between the mechanical and electrical properties (i.e., elasticity and conductivity, respectively). The composite hydrogel G' exhibited three regions (strong, transition, weak) and was significantly reduced at PEDOT:PSS concentrations above 0.4 wt %. For PEDOT:PSS concentrations below 0.4 wt %,

increasing PEDOT:PSS concentration caused an increase in conductivity and a decrease in electrical impedance but had relatively little effect on the hydrogel elasticity. For PEDOT:PSS concentrations above 0.45 wt %, increasing PEDOT:PSS concentration caused continued conductivity increase but at a relatively lower rate of change while the elasticity (i.e., G') remained relatively constant. However, between the two regions (i.e., 0.4-0.45 wt %), G' underwent a sharp change, specifically, a significant decrease with respect to increasing PEDOT:PSS concentration. Benchmarking of the electrical impedance response obtained using a network analyzer vs potentiostat is shown in Figure 6F with the associated material conductivity (Bode plots associated with potentiostatic EIS data are shown in Figure S3A). The measured resistance of the samples also exhibited a trend similar to that of the electrical impedance data (Figure S3B). The multiproperty HTC data show a clear trade-off between mechanical and electrical properties and can be used to identify an optimized formulation for device manufacturing. For example, while the conductive functional composite hydrogel may be relatively more conductive above PE-DOT:PSS concentrations of 0.45 wt %, it exhibits poor mechanical properties. Thus, we selected a PEDOT:PSS concentration of 0.4 wt %, the concentration that precedes the sharp decrease in mechanical properties, as an optimized formulation for subsequent device fabrication via additive manufacturing. Thus, the selection of the optimized formulation here was based on the generated compositionproperty relations in combination with imposed thresholds on material property-based critical quality attributes. Figure 6G,H shows photographs of 3D-printed PEGDMA/PEDOT:PSS composite hydrogel constructs in the shape of a Virginia Tech ("VT") logo containing integrated LEDs. The minimum voltages required to generate light visible with the naked eye for the two circuits were approximately 4.5 and 14 V, respectively. Composite hydrogels of PEGDA/PEDOT have many potential applications, including bioelectronics. 53-58 These applications require the composite material to exhibit suitable mechanical and electrical properties, which can be identified via HTE-based accelerated materials optimization.

Considering material optimization applications of the HTE method, which was the focus of this work, existing composition-process-property data from previous studies can provide design constraints for the formulation (e.g., concentration limits for specific mixture components). However, for material discovery applications in which the composition-property relations may not yet have been investigated for many materials, the HTE method can leverage knowledge generated by initial manual experimentation to avoid blind investigation of the material design space (i.e., the composition-process parameter space). For example, traditional experimentation may identify limits on the reagent composition (e.g., formulations that do not solidify). Active learning is also increasingly used to guide HTE processes for accelerated material discovery and optimization applications to overcome the challenges associated with blind exploration of the formulation-process parameter design spaces in cases with limited prior knowledge and complex material systems. In this work, the experimental design was constrained and guided by prior knowledge of the material system's phase behavior, processability (e.g., minimal dispensing volume), sensor characteristics (e.g., detection limit), sample number associated with well plate formats, and property of interest to be

optimized, which here was most typically the mechanical property. Beyond high-throughput mechanical property characterization, other high-throughput characterization measurements, such as the multiproperty characterization of optical and electrical properties, assisted in understanding the mechanical property-composition relation. For example, the change of absorbance of the alginate/PNIPAM material helped to understand the percolation of the interpenetrated polymer network as well as the trend in the mechanical propertycomposition relation observed by the cantilever sensor data (i.e., phase angle response).

### 4. CONCLUSIONS

This work was driven by the demand for accelerated engineering (e.g., optimization) of soft functional materials, particularly hydrogels, which are used extensively. There remains a need for HTE formats that synergize with multiproperty HTC methods for accelerated engineering of functional composite hydrogels with optimized processability and performance, particularly in practical cross-disciplinary formats, such as well plates, that are used extensively in HTE applications. We demonstrated an HTE method based on integrated robotically directed dispensing and sensing that synergizes with well plate formats. The method was leveraged to identify formulations of several functional composite hydrogels that exhibit optimized processability and performance. Limitations of the method are rooted in the performance constraints of the underlying dispensing and sensing tools. Thus, the performance of the HTE method can be improved in future work with advances in the underlying processes and tools (e.g., parameter selection, path planning, and sensing). In application to other material systems, one may consider material availability (sample size limitations) and solubility, which may constrain the concentration range investigated. Material selection may also be constrained by material processability (e.g., extrudability and miscibility). The concentration range may also be constrained by the relationship of the material's properties with respect to the dynamic range of the utilized characterization tools (e.g., detection limit). Future opportunities include application to continuous monitoring of hydrogel dynamic processes (e.g., gelation and stimuli-response), understanding temperature dependence of material properties, integration with digital twin, and incorporation into data-driven decision-making. The ultimate goal is to utilize the generated HTC data to establish autonomous closed-loop HTE formats that can operate with minimal resource expenditures and human intervention.

# **ASSOCIATED CONTENT**

#### Supporting Information

The Supporting Information is available free of charge at https://pubs.acs.org/doi/10.1021/acsami.3c11483.

Additional description of the fluid-structure interaction model for the dynamic-mode cantilever sensor, photographs of sensors and mixers, results of senor stability testing, additional supporting impedimetric data generated during HTC, and characterization of solution viscosity (PDF)

#### AUTHOR INFORMATION

# **Corresponding Author**

Blake N. Johnson — Grado Department of Industrial and Systems Engineering, Virginia Tech, Blacksburg, Virginia 24061, United States; Macromolecules Innovation Institute, Department of Materials Science and Engineering, and Department of Chemical Engineering, Virginia Tech, Blacksburg, Virginia 24061, United States; orcid.org/0000-0003-4668-2011; Phone: 540-231-0755; Email: bnj@vt.edu; Fax: 540-231-3322

#### **Authors**

- Yang Liu Grado Department of Industrial and Systems Engineering, Virginia Tech, Blacksburg, Virginia 24061, United States; Macromolecules Innovation Institute, Virginia Tech, Blacksburg, Virginia 24061, United States
- Junru Zhang Grado Department of Industrial and Systems Engineering, Virginia Tech, Blacksburg, Virginia 24061, United States
- Yujing Zhang Bradley Department of Electrical and Computer Engineering, Virginia Tech, Blacksburg, Virginia 24061, United States
- Hu Young Yoon Macromolecules Innovation Institute and Department of Sustainable Biomaterials, Virginia Tech, Blacksburg, Virginia 24061, United States; ◎ orcid.org/ 0000-0001-8841-4758
- Xiaoting Jia Bradley Department of Electrical and Computer Engineering, Virginia Tech, Blacksburg, Virginia 24061, United States; orcid.org/0000-0003-4890-6103
- Maren Roman − Macromolecules Innovation Institute and Department of Sustainable Biomaterials, Virginia Tech, Blacksburg, Virginia 24061, United States; orcid.org/0000-0001-6622-8591

Complete contact information is available at: https://pubs.acs.org/10.1021/acsami.3c11483

#### Notes

The authors declare no competing financial interest.

# ACKNOWLEDGMENTS

This work was supported by GlycoMIP, a National Science Foundation Materials Innovation Platform funded through Cooperative Agreement DMR-1933525. B.N.J. is also grateful for the generous support of the National Science Foundation awards CMMI-2141008 and CMMI-2126176, which provided partial support for this work. X.J. gratefully acknowledges funding support from the National Science Foundation (ECCS-1847436) and the US National Institutes of Health (R01NS123069 and R21EY033080).

# REFERENCES

- (1) Green, M. L.; Choi, C. L.; Hattrick-Simpers, J. R.; Joshi, A. M.; Takeuchi, I.; Barron, S. C.; Campo, E.; Chiang, T.; Empedocles, S.; Gregoire, J. M.; et al. Fulfilling The Promise of The Materials Genome Initiative With High-Throughput Experimental Methodologies. *Appl. Phys. Rev.* **2017**, *4* (1), No. 011105.
- (2) Mennen, S. M.; Alhambra, C.; Allen, C. L.; Barberis, M.; Berritt, S.; Brandt, T. A.; Campbell, A. D.; Castanon, J.; Cherney, A. H.; Christensen, M.; et al. The Evolution of High-Throughput Experimentation in Pharmaceutical Development and Perspectives on the Future. Org. Process Res. Dev. 2019, 23 (6), 1213–1242.
- (3) Green, M. L.; Takeuchi, I.; Hattrick-Simpers, J. R. Applications of High Throughput (Combinatorial) Methodologies to Electronic,

- Magnetic, Optical, and Energy-Related Materials. J. Appl. Phys. 2013, 113 (23), No. 231101.
- (4) Kumachev, A.; Greener, J.; Tumarkin, E.; Eiser, E.; Zandstra, P. W.; Kumacheva, E. High-Throughput Generation of Hydrogel Microbeads With Varying Elasticity for Cell Encapsulation. *Biomaterials* **2011**, 32 (6), 1477–1483.
- (5) Domachuk, P.; Tsioris, K.; Omenetto, F. G.; Kaplan, D. L. Biomicrofluidics: Biomaterials and Biomimetic Designs. *Adv. Mater.* **2010**, 22 (2), 249–260.
- (6) Barata, D.; van Blitterswijk, C.; Habibovic, P. High-Throughput Screening Approaches and Combinatorial Development of Biomaterials Using Microfluidics. *Acta Biomater.* **2016**, *34*, 1–20.
- (7) Zhang, R.; Liberski, A.; Khan, F.; Diaz-Mochon, J. J.; Bradley, M. Inkjet Fabrication of Hydrogel Microarrays Using in situ Nanolitre-Scale Polymerisation. *Chem. Commun.* **2008**, No. 11, 1317–1319.
- (8) Zhang, R.; Liberski, A.; Sanchez-Martin, R.; Bradley, M. Microarrays of Over 2000 Hydrogels Identification of Substrates for Cellular Trapping and Thermally Triggered Release. *Biomaterials* **2009**, *30* (31), 6193–6201.
- (9) Rosenfeld, A.; Oelschlaeger, C.; Thelen, R.; Heissler, S.; Levkin, P. A. Miniaturized High-Throughput Synthesis and Screening of Responsive Hydrogels Using Nanoliter Compartments. *Materials Today Bio* **2020**, *6*, No. 100053.
- (10) Ranga, A.; Gobaa, S.; Okawa, Y.; Mosiewicz, K.; Negro, A.; Lutolf, M. P. 3D Niche Microarrays for Systems-Level Analyses of Cell Fate. *Nat. Commun.* **2014**, *5* (1), No. 4324.
- (11) Yang, Y.-H.; Khan, Z.; Ma, C.; Lim, H. J.; Smith Callahan, L. A. Optimization of Adhesive Conditions for Neural Differentiation of Murine Embryonic Stem Cells Using Hydrogels Functionalized With Continuous Ile-Lys-Val-Ala-Val Concentration Gradients. *Acta Biomater.* **2015**, 21, 55–62.
- (12) Guimarães, C. F.; Gasperini, L.; Ribeiro, R. S.; Carvalho, A. F.; Marques, A. P.; Reis, R. L. High-Throughput Fabrication of Cell-Laden 3D Biomaterial Gradients. *Mater. Horiz.* **2020**, *7* (9), 2414–2421.
- (13) Xu, F.; Corbett, B.; Bell, S.; Zhang, C. Y.; Hartono, M. B.; Farsangi, Z. J.; MacGregor, J.; Hoare, T. High-Throughput Synthesis, Analysis, and Optimization of Injectable Hydrogels for Protein Delivery. *Biomacromolecules* **2020**, *21* (1), 214–229.
- (14) Ding, Y.; Tang, H. Q.; Zhang, C. H.; Li, W. X.; Li, G.; Zhang, Y.; Xu, C.; Zhao, F.; Guo, Q. Y.; Guo, C. F.; Xiang, X. High-Throughput Screening of Self-Healable Polysulfobetaine Hydrogels and their Applications in Flexible Electronics. *Adv. Funct. Mater.* **2021**, *31* (18), No. 2100489.
- (15) Zhang, J.; Liu, Y.; Chandra Sekhar P, D.; Singh, M.; Tong, Y.; Kucukdeger, E.; Yoon, H. Y.; Haring, A. P.; Roman, M.; Kong, Z.; Johnson, B. N. Rapid, Autonomous High-Throughput Characterization of Hydrogel Rheological Properties via Automated Sensing and Physics-Guided Machine Learning. *Appl. Mater. Today* **2023**, *30*, No. 101720.
- (16) de Rutte, J. M.; Koh, J.; Di Carlo, D. Scalable High-Throughput Production of Modular Microgels for In Situ Assembly of Microporous Tissue Scaffolds. *Adv. Funct. Mater.* **2019**, 29 (25), 10.
- (17) Wang, M.; Nai, M. H.; Huang, R. Y.-J.; Leo, H. L.; Lim, C. T.; Chen, C.-H. High-Throughput Functional Profiling of Single Adherent Cells via Hydrogel Drop-Screen. *Lab Chip* **2021**, *21* (4), 764–774
- (18) André, E.; Pannacci, N.; Dalmazzone, C.; Colin, A. A New Way to Measure Viscosity in Droplet-Based Microfluidics for High Throughput Analysis. *Soft Matter* **2019**, *15* (3), 504–514.
- (19) Oevreeide, I. H.; Szydlak, R.; Luty, M.; Ahmed, H.; Prot, V.; Skallerud, B. H.; Zemla, J.; Lekka, M.; Stokke, B. T. On the Determination of Mechanical Properties of Aqueous Microgels-Towards High-Throughput Characterization. *Gels* **2021**, *7* (2), No. 64.
- (20) Marquez, J. P.; Legant, W.; Lam, V.; Cayemberg, A.; Elson, E.; Wakatsuki, T. High-Throughput Measurements of Hydrogel Tissue Construct Mechanics. *Tissue Eng., Part C* **2009**, *15* (2), 181–190.

- (21) Haring, A. P.; Singh, M.; Koh, M.; Cesewski, E.; Dillard, D. A.; Kong, Z. J.; Johnson, B. N. Real-Time Characterization of Hydrogel Viscoelastic Properties and Sol-Gel Phase Transitions Using Cantilever Sensors. *J. Rheol.* **2020**, *64* (4), 837–850.
- (22) Cesewski, E.; Singh, M.; Liu, Y.; Zhang, J.; Haring, A. P.; Johnson, B. N. Real-Time Monitoring of Hydrogel Rheological Property Changes and Gelation Processes Using High-Order Modes of Cantilever Sensors. *J. Appl. Phys.* **2020**, *128* (17), No. 174502.
- (23) Singh, M.; Zhang, J.; Bethel, K.; Liu, Y.; Davis, E. M.; Zeng, H.; Kong, Z.; Johnson, B. N. Closed-Loop Controlled Photopolymerization of Hydrogels. ACS Appl. Mater. Interfaces 2021, 13 (34), 40365–40378.
- (24) Liu, Y.; Bethel, K.; Singh, M.; Zhang, J.; Ashkar, R.; Davis, E. M.; Johnson, B. N. Comparison of Bulk- vs Layer-by-Layer-Cured Stimuli-Responsive PNIPAM—Alginate Hydrogel Dynamic Viscoelastic Property Response via Embedded Sensors. ACS Appl. Polym. Mater. 2022. 4 (8), 5596—5607.
- (25) Johnson, B. N.; Mutharasan, R. Persistence of Bending and Torsional Modes in Piezoelectric-Excited Millimeter-Sized Cantilever (PEMC) Sensors in Viscous Liquids 1 to 103 cP. *J. Appl. Phys.* **2011**, 109 (6), No. 066105.
- (26) Haring, A. P.; Khan, A. U.; Liu, G.; Johnson, B. N. 3D Printed Functionally Graded Plasmonic Constructs. *Adv. Opt. Mater.* **2017**, 5 (18), No. 1700367.
- (27) Killion, J. A.; Geever, L. M.; Devine, D. M.; Kennedy, J. E.; Higginbotham, C. L. Mechanical Properties and Thermal Behaviour of PEGDMA Hydrogels for Potential Bone Regeneration Application. *J. Mech. Behav. Biomed. Mater.* **2011**, 4 (7), 1219–1227.
- (28) Burke, G.; Barron, V.; Geever, T.; Geever, L.; Devine, D. M.; Higginbotham, C. L. Evaluation of the Materials Properties, Stability and Cell Response of a Range of PEGDMA Hydrogels for Tissue Engineering Applications. *J. Mech. Behav. Biomed. Mater.* **2019**, 99, 1–10.
- (29) de Lima, G. G.; Elter, J. K.; Chee, B. S.; Magalhaes, W. L. E.; Devine, D. M.; Nugent, M. J. D.; de Sa, M. J. C. A Tough and Novel Dual-Response PAA/P(NiPAAM-co-PEGDMA) IPN Hydrogels With Ceramics by Photopolymerization for Consolidation of Bone Fragments Following Fracture. *Biomed. Mater.* **2019**, *14* (5), No. 054101.
- (30) Mather, M. L.; Rides, M.; Allen, C. R. G.; Tomlins, P. E. Liquid Viscoelasticity Probed by a Mesoscale Piezoelectric Bimorph Cantilever. *J. Rheol.* **2012**, *56* (1), 99–112.
- (31) Yang, J.; Han, C.-R.; Duan, J.-F.; Ma, M.-G.; Zhang, X.-M.; Xu, F.; Sun, R.-C.; Xie, X.-M. Studies on the Properties and Formation Mechanism of Flexible Nanocomposite Hydrogels From Cellulose Nanocrystals and Poly(acrylic acid). *J. Mater. Chem.* **2012**, 22 (42), 22467–22480.
- (32) Yang, J.; Han, C.-R. Dynamics of Silica-Nanoparticle-Filled Hybrid Hydrogels: Nonlinear Viscoelastic Behavior and Chain Entanglement Network. *J. Phys. Chem. C* **2013**, *117* (39), 20236–20243.
- (33) Linke, J.; Fazio, M. A.; Cavalcoli, D.; Terheiden, B. Multi-Characterization Study of Interface Passivation Quality of Amorphous Sub-Stoichiometric Silicon Oxide and Silicon Oxynitride Layers for Photovoltaic Applications. *Sol. Energy Mater. Sol. Cells* **2018**, *187*, 104–112.
- (34) Wu, J. X.; Yang, S.; Cai, W.; Bi, Z. F.; Shang, G. Y.; Yao, J. N. Multi-Characterization of LiCoO2 Cathode Films Using Advanced AFM-Based Techniques With High Resolution. *Sci. Rep.* **2017**, *7*, No. 11164.
- (35) Abbas, A.; Vivien, C.; Bocquet, B.; Guillochon, D.; Supiot, P. Preparation and Multi-Characterization of Plasma Polymerized Allylamine Films. *Plasma Process Polym.* **2009**, *6* (9), 593–604.
- (36) Chen, Q.; Chen, H.; Zhu, L.; Zheng, J. Fundamentals of Double Network Hydrogels. J. Mater. Chem. B 2015, 3 (18), 3654–3676
- (37) Zhou, Y.; Wan, C.; Yang, Y.; Yang, H.; Wang, S.; Dai, Z.; Ji, K.; Jiang, H.; Chen, X.; Long, Y. Highly Stretchable, Elastic, and Ionic

- Conductive Hydrogel for Artificial Soft Electronics. *Adv. Funct. Mater.* **2019**, 29 (1), No. 1806220.
- (38) Tang, S.; Yang, J.; Lin, L.; Peng, K.; Chen, Y.; Jin, S.; Yao, W. Construction of Physically Crosslinked Chitosan/Sodium Alginate/Calcium Ion Double-Network Hydrogel and Its Application to Heavy Metal Ions Removal. *Chem. Eng. J.* **2020**, 393, No. 124728.
- (39) Wiener, C. G.; Wang, C.; Liu, Y.; Weiss, R. A.; Vogt, B. D. Nanostructure Evolution During Relaxation From a Large Step Strain in a Supramolecular Copolymer-Based Hydrogel: A SANS Investigation. *Macromolecules* **2017**, *50* (4), 1672–1680.
- (40) Yu, L.; Yakubov, G. E.; Gilbert, E. P.; Sewell, K.; van de Meene, A. M. L.; Stokes, J. R. Multi-Scale Assembly of Hydrogels Formed by Highly Branched Arabinoxylans From Plantago Ovata Seed Mucilage Studied by USANS/SANS and Rheology. *Carbohydr. Polym.* **2019**, 207, 333–342.
- (41) Nishi, K.; Shibayama, M. Probe-SAXS on Hydrogels Under Elongation. *Soft Matter* **2016**, *12* (24), 5334–5339.
- (42) Huang, L.; Ding, L.; Zhou, J.; Chen, S.; Chen, F.; Zhao, C.; Xu, J.; Hu, W.; Ji, J.; Xu, H.; Liu, G. L. One-step Rapid Quantification of SARS-CoV-2 Virus Particles via Low-Cost Nanoplasmonic Sensors in Generic Microplate Reader and Point-of-Care Device. *Biosens. Bioelectron.* 2021, 171, No. 112685.
- (43) Mauri, M.; Vecchione, S.; Fritz, G. Deconvolution of Luminescence Cross-Talk in High-Throughput Gene Expression Profiling. ACS Synth. Biol. 2019, 8 (6), 1361–1370.
- (44) Yeow, J.; Joshi, S.; Chapman, R.; Boyer, C. A Self-Reporting Photocatalyst for Online Fluorescence Monitoring of High Throughput RAFT Polymerization. *Angew. Chem., Int. Ed.* **2018**, *57* (32), 10102–10106.
- (45) Nakamura, T.; Mizukami, S.; Tanaka, M.; Kikuchi, K. Efficient Formation of Luminescent Lanthanide(III) Complexes by Solid-Phase Synthesis and On-Resin Screening. *Chem. Asian J.* **2013**, 8 (11), 2685–2690.
- (46) Rahaman, M.; Aldalbahi, A.; Govindasami, P.; Khanam, N. P.; Bhandari, S.; Feng, P.; Altalhi, T. A New Insight in Determining the Percolation Threshold of Electrical Conductivity for Extrinsically Conducting Polymer Composites Through Different Sigmoidal Models. *Polymers* **2017**, *9* (10), 527.
- (47) Moud, A. A.; Kamkar, M.; Sanati-Nezhad, A.; Hejazi, S. H.; Sundararaj, U. Viscoelastic Properties of Poly (vinyl alcohol) Hydrogels With Cellulose Nanocrystals Fabricated Through Sodium Chloride Addition: Rheological Evidence of Double Network Formation. *Colloids Surf., A* **2021**, *609*, No. 125577.
- (48) Duan, Y.; Zhao, Y.; Ai, S.; Qiu, D.; Wang, X.; Qu, X.; Yang, Z. Programmable Processing Toward Stiff Composite Hydrogels. *Macromolecules* **2022**, *55* (16), 7071–7079.
- (49) Kayser, L. V.; Lipomi, D. J. Stretchable Conductive Polymers and Composites Based on PEDOT and PEDOT:PSS. *Adv. Mater.* **2019**, *31* (10), No. 1806133.
- (50) Sun, K.; Zhang, S.; Li, P.; Xia, Y.; Zhang, X.; Du, D.; Isikgor, F. H.; Ouyang, J. Review on Application of PEDOTs and PEDOT:PSS in Energy Conversion and Storage Devices. *J. Mater. Sci.: Mater. Electron.* **2015**, 26 (7), 4438–4462.
- (51) Fan, X.; Nie, W.; Tsai, H.; Wang, N.; Huang, H.; Cheng, Y.; Wen, R.; Ma, L.; Yan, F.; Xia, Y. PEDOT:PSS for Flexible and Stretchable Electronics: Modifications, Strategies, and Applications. *Adv. Sci.* **2019**, *6* (19), No. 1900813.
- (52) Kaur, G.; Adhikari, R.; Cass, P.; Bown, M.; Gunatillake, P. Electrically Conductive Polymers and Composites for Biomedical Applications. *RSC Adv.* **2015**, 5 (47), 37553–37567.
- (53) Heo, D. N.; Lee, S.-J.; Timsina, R.; Qiu, X.; Castro, N. J.; Zhang, L. G. Development of 3D Printable Conductive Hydrogel With Crystallized PEDOT:PSS for Neural Tissue Engineering. *Mater. Sci. Eng., C* **2019**, *99*, 582–590.
- (54) Guex, A. G.; Puetzer, J. L.; Armgarth, A.; Littmann, E.; Stavrinidou, E.; Giannelis, E. P.; Malliaras, G. G.; Stevens, M. M. Highly Porous Scaffolds of PEDOT:PSS for Bone Tissue Engineering. *Acta Biomater.* **2017**, *62*, 91–101.

- (55) Khalili, A.; Noziere, R.; Tuberty-Vaughan, E.; Freeman, J. W. Self-Actuating Multilayer Scaffold for Skeletal Muscle Tissue Engineering. *Polym. Adv. Technol.* **2022**, 33 (10), 3228–3237.
- (56) Abdullah, H.; Phairatana, T. A Study on the Performances of PEGDA and PEDOT: PSS Composite Resin for 3D-Printed Biosensor Applications. ECS Trans. 2022, 107 (1), 15001.
- (57) Lopez-Larrea, N.; Criado-Gonzalez, M.; Dominguez-Alfaro, A.; Alegret, N.; Agua, Id.; Marchiori, B.; Mecerreyes, D. Digital Light 3D Printing of PEDOT-Based Photopolymerizable Inks for Biosensing. ACS Appl. Polym. Mater. 2022, 4 (9), 6749–6759.
- (58) Polino, G.; Lubrano, C.; Scognamiglio, P.; Mollo, V.; De Martino, S.; Ciccone, G.; Matino, L.; Langella, A.; Netti, P.; Di Carlo, A.; et al. Synthesis and Characterization of PEDOT-PEGDA Blends for Bioelectronic Applications: Surface Properties and Effects on Cell Morphology. Flex. Print. Electron. 2020, 5 (1), No. 014012.